Analysis of Critical Excavation Depth for a Jointed Rock Slope Using a Face-to-Face Discrete Element Method

By

S. H. Li[1], **J. G. Wang**[2], **B. S. Liu**[1], and **D. P. Dong**[1]

[1] Institute of Mechanics, Chinese Academy of Science, Beijing, P.R. China
[2] Tropical Marine Science Institute, National University of Singapore, Singapore

Summary

The critical excavation depth of a jointed rock slope is an important problem in rock engineering. This paper studies the critical excavation depth for two idealized jointed rock slopes by employing a face-to-face discrete element method (DEM). The DEM is based on the discontinuity analysis which can consider anisotropic and discontinuous deformations due to joints and their orientations. It uses four lump-points at each surface of rock blocks to describe their interactions. The relationship between the critical excavation depth D_s and the natural slope angle α, the joint inclination angle θ as well as the strength parameters of the joints c_r, ϕ_r is analyzed, and the critical excavation depth obtained with this DEM and the limit equilibrium method (LEM) is compared. Furthermore, effects of joints on the failure modes are compared between DEM simulations and experimental observations. It is found that the DEM predicts a lower critical excavation depth than the LEM if the joint structures in the rock mass are not ignored.

Keywords: Slope stability, discontinuity, critical excavation depth, face-to-face DEM, limit equilibrium method, joint configuration.

1. Introduction

The excavation of jointed rock slopes may cause landslides and interrupt construction. Thus slope stability is always a concern during excavation and the maximum excavation depth or critical excavation depth is often the focus. The limit equilibrium method (LEM) is widely used in the stability analysis of rock slopes (Duncan, 1996; Wang et al., 2004). It can also be used to get the critical excavation depth. In the LEM, a sliding surface is assumed to be formed along the weakest layer of shear resistance which may be obtained through a searching routine (Low et al., 1998). The factor of safety, which is used to evaluate the stability of a slope, is defined as the ratio of the

resisting force to the sliding force along the sliding surface. The concept of the LEM is simple and practical, and abundant experience has been accumulated in practice (Chen et al., 2001; Kentli and Topal, 2004; Kim et al., 2004). However, the LEM cannot consider the effects of stress and deformation distribution nor multiple structural interfaces such as joints and fissures in a sliding body (Li et al., 2005). In order to consider these factors, several numerical methods have been proposed in rock mechanics (see review papers by Jing (2003); Jiang and Hudson (2002)), and the discrete element method (DEM) is one of promising methods for stability analysis of jointed rock slopes (Dowding et al., 1983; Lu et al., 2002; Chen and Li, 2004).

The DEM was first proposed by Cundall (1971) to study the movements of granular assemblies (Cundall and Strack, 1979). This method was coded into a computer software, UDEC (Board, 1989) which was based on a two-dimensional vertex-to-face model. Being different from the Cundall's vertex-to-face model, Dowding (1983) proposed a face-to-face model to consider the structural interfaces in rock masses. This face-to-face model constrains the orientation of contact forces, avoiding the difficulty of the vertex-to-face model in the determination of the direction of contact forces. It is more reliable and much simpler to search for the contacts in discrete blocks when displacements are small. This can reduce computation cost (O'Conner and Dowding, 1992; Dowding et al., 1999; 2000). The face-to-face DEM (called DEM hereafter) was successfully applied to jointed rock masses in engineering. For example, O'Connor and Dowding (1992) applied the 3D-DEM model to analyze mining-induced subsidence. In recent years, this face-to-face DEM has been extended to include a hexahedral element (Chen and Li, 2004) and applied to the slope stability analysis of the Three Gorges project (Lu et al., 2002) and blasting-induced rock mass vibration (Guo and Li, 2002).

Joint structures play critical roles in the stability of a jointed rock slope during excavation (Cook, 1992; Gokceoglu et al., 2000; Yoon et al., 2002). However, the relationship between joint structures in a rock mass and the factor of safety of a jointed rock slope is not clear so far. This paper will study the effect of joint structures on the critical excavation depth for two typical jointed rock slopes through the face-to-face 3D DEM model. The relationship between slope stability and slope parameters such as slope geometry, joint structure and joint strength is numerically studied. The DEM simulations are compared with the LEM closed-form solutions and the LEM numerical results. The failure modes for a rock slope with different joint structures are experimentally observed and numerically simulated with the DEM. It is found that joints both along the sliding surface and in the sliding body may affect the critical excavation depth and that the DEM may predict a lower critical excavation depth than the LEM.

2. Fundamentals of the Face-to-Face Model

Rock masses can be divided into blocks according to joint orientations and their spatial distribution. The DEM model in this study involves three primary sets of joints which cut the rock mass into hexahedron blocks as shown in Fig. 1. The blocks contact each other at the interface or block surface to form a face-to-face model. Each surface defines four points (called lump points) to transfer the forces on this surface.
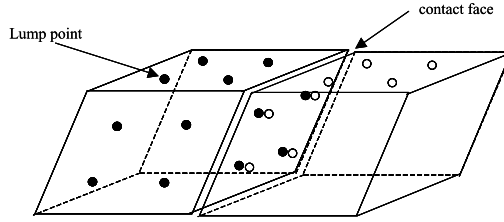
Fig. 1. Face-to-face model and positions of lump points

Therefore, these lump points are the acting points of the forces between two adjacent blocks. Each block has two external forces: body forces and contacting forces from neighboring blocks. Based on Newton's second law, the equation of motion of the ith block is expressed as follows:

$$m_i \ddot{\vec{u}}_i + c_m \dot{\vec{u}}_i + c_k \sum_{j=1}^{n} (\dot{\vec{u}}_i - \dot{\vec{u}}_j) + k \sum_{j=1}^{n} (\vec{u}_i - \vec{u}_j) = \vec{F} \tag{1}$$

and

$$I_i \ddot{\vec{\theta}}_i + c_I r_0^2 \dot{\vec{\theta}}_i + c_k \sum_{k=1}^{n'} \{\vec{r}_k \times [\vec{r}_k \times (\dot{\vec{\theta}}_i - \dot{\vec{\theta}}_j)]\} + k \sum_{k=1}^{n'} \{\vec{r}_k \times [\vec{r}_k \times (\vec{\theta}_i - \vec{\theta}_j)]\} = \vec{M}, \tag{2}$$

where m_i and I_i are the mass and the moment of inertia of the ith block, respectively, $\vec{u}_i$, $\dot{\vec{u}}_i$, $\ddot{\vec{u}}_i$, $\vec{\theta}_i$, $\dot{\vec{\theta}}_i$, $\ddot{\vec{\theta}}_i$ are displacement, velocity, acceleration, angular displacement, angular velocity, and angular acceleration, respectively. The subscript 'j' refers to the jth-neighboring block. n is the block number which is adjacent to the ith block, and n' the lump points on the ith block. $\vec{F}$ is the external force such as gravity, and $\vec{M}$ the external moment. r_0 is the rotating radius and $\vec{r}_k$ the vector from the block mass center to lump points. c_I, c_m, c_k, k are physical constants.

At each lump point, the normal force F_n and the shear force F_s, which express the interaction between two adjacent blocks, are expressed as (Wang et al., 2003):

$$F_n = -k_n \Delta u_n, \quad F_s = -k_s \Delta u_s \tag{3}$$

where Δu_n and Δu_s are the relative normal and shear displacements, respectively. k_n and k_s are the normal and shear stiffnesses.

The criteria of failure at each lump point are as follows:

$$F_n = 0, \quad F_s = 0, \quad \text{when} \quad \frac{F_n}{S} \geq \sigma_t \tag{4}$$

$$F_s = F_n \tan \phi_r + C \quad \text{when} \quad \frac{F_s}{S} \geq c_r + \frac{F_n}{S} \tan \phi_r, \tag{5}$$

where S is the area acted on by forces F_n and F_s. $c_r = C/S$ the cohesion, and ϕ_r the friction angle of the joints. σ_t is the tensile strength. When the normal stress at this lump point is greater than σ_t, the blocks detach and the future tensile strength is set as zero.

The dynamic relaxation method is used for time integration. Forces and displacements are updated in each computing cycle, and the computation is iterated in each

time step. The calculation ends when the kinetic energy converges to zero or a non-zero value.

3. Critical Excavation Depth for a Typical Jointed Rock Slope

3.1 Geometry Model

Figure 2 is a typical jointed rock slope. Its dimensions are $X_L = 50$ m, $Y_L = 70$ m, and $Z_L = 50 \tan \alpha + 10$(m), respectively. For convenience, three sets of joints with spacing of 2 m cut the rock masses into quasi-3D blocks. The parameters for these three sets of joints are shown in Fig. 2(a). They are $\psi_1 = 90°$, $\theta_1 = \theta$; $\psi_2 = 90°$, $\theta_2 = 90° - \theta$ and $\psi_3 = 0°$, $\theta_3 = 90°$, where θ is the dip angle of plane AC in Fig. 2(b).

3.2 Criterion for Slope Stability

A block will slide if the shear strength between two adjacent rock blocks cannot resist the sliding forces imposed by other adjacent blocks. When all sliding surfaces connect each other to form a continuous surface and this continuous surface goes through the slope borders, the unstable mass of this slope will move with a constant velocity or acceleration. At this time, the kinetic energy of the slope is non-zero. Therefore, a slope is not stable if the velocities of some blocks cannot converge to zero. On the other hand, a stable slope should have zero kinetic energy. In our DEM computation, we regard the convergence of kinetic energy to zero as the criterion for slope stability.

3.3 Critical Excavation Depth Calculated by the LEM

The typical rock slope as shown in Fig. 2(b) has a plane sliding surface. The unstable mass is a triangular prism ΔABC. It is defined by the following geometrical
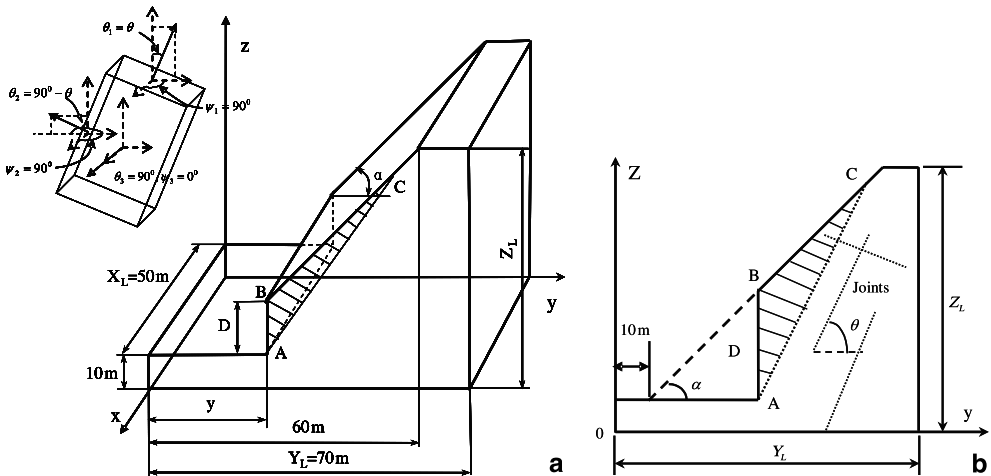

Fig. 2a, b. Schematic excavation of a jointed rock slope. **a** Three-dimensional view, **b** two-dimensional view

parameters: the natural slope angle α, the joint inclination angle θ and the excavation depth D. The sectional area of this prism is:

$$S_{\triangle ABC} = f(\alpha, \theta, D) = \frac{1}{2} \frac{D^2}{\tan\theta - \tan\alpha}. \tag{6}$$

If the unit weight of this slope is γ, the weight of this triangular prism in unit length is:

$$G = \gamma S_{\triangle ABC} = \frac{1}{2}\gamma \frac{D^2}{\tan\theta - \tan\alpha}. \tag{7}$$

Its factor of safety is obtained as:

$$
\begin{aligned}
F &= \frac{\text{Shear strength}}{\text{Shear force}} = \frac{c_r D}{G\sin\theta(\sin\theta - \cos\theta\tan\alpha)} + \frac{\tan\phi_r}{\tan\theta} \\
&= \frac{2c_r}{\gamma D\sin\theta\cos\theta} + \frac{\tan\phi_r}{\tan\theta},
\end{aligned}
\tag{8}
$$

where ϕ_r is the friction angle and c_r the cohesion along the sliding surface. It is noted that the critical excavation depth D_s is the excavation depth D when the slope is in its critical state, that is $F = 1$. From Eq. (8) this D_s can be obtained as

$$D_s = g(\theta, \gamma, c_r, \phi_r) = \frac{2c_r}{\gamma\cos^2\theta(\tan\theta - \tan\phi_r)}. \tag{9}$$

It is noted that Eq. (9) is meaningful only if $\theta > \phi_r$. If $\theta \leq \phi_r$, the excavated slope will never slide along the joint surface unless additional forces are imposed or strength in the joint surface is lost (Wei et al., 2005). Furthermore, Eq. (9) does not consider the effect of joints inside the sliding mass because the LEM regards the triangular sliding mass as rigid. This closed-form of critical excavation depth is only applicable to the case in which slope sliding is controlled by only one set of joints along the sliding surface. If slope sliding is controlled by more than one set of joints, closed-form solutions are usually not available, and the DEM simulation is usually employed to investigate the effect of joints.

4. Numerical Simulations with DEM and Discussion

4.1 Graphs of Sliding Blocks and Displacements

In order to compare the above LEM closed-form solution with the DEM simulation, the slope is assumed to slide along one joint surface only. We evaluate the slope stability with different excavation depths and monitor the displacements until the slope fails. The following parameters are used in the computation: the natural slope angle $\alpha = 45°$ and the joint inclination angle $\theta = 65°$. The strength parameters of joints are $\phi_r = 30°$, $c_r = 0.13\,\text{MPa}$ and $\sigma_t = 0.6\,\text{MPa}$. The strength parameters of intact rock are $\phi_r = 50°$, $c_r = 0.60\,\text{MPa}$ and $\sigma_t = 0.6\,\text{MPa}$, and the density of rock mass is $\gamma = 26.46\,\text{kN/m}^3$. Figure 3 shows the typical displacements at the point of $x_0 = 24.5\,\text{m}$, $y_0 = 47.5\,\text{m}$, and $z_0 = 46.3\,\text{m}$ when excavation depths vary from 0 to 35 m. It is found that the displacements increase rapidly after the excavation depth exceeds 30 m. All blocks inside
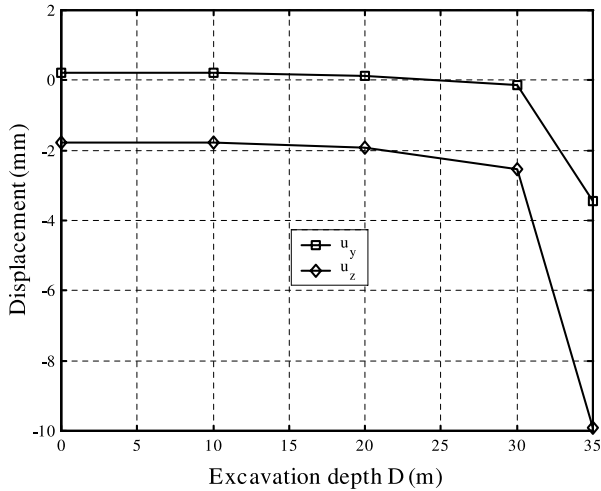
Fig. 3. Variation of block displacement with excavation depth D

the sliding triangular area show the same sliding trend. When the excavation depth reaches 35 m, the displacements increase without limit, which corresponds to sliding failure. Figure 4(a) and (b) show the distributions of block mass centers and slip points at two excavation depths, 30 m and 35 m. When the excavation depth is 30 m as shown in Fig. 4(a), slip points occur in the upper part but have not gone through the slope to form a sliding surface. This indicates that the slope has not achieved its critical state. When the excavation depth reaches 35 m, the slip points almost form a sliding surface as shown in Fig. 4(b), and the slope is in its critical state and slides. The sliding mass is exactly a triangular prism.

4.2 Effect of Excavation Procedures

It is noted that the above DEM simulations are carried out through a vertical column excavation procedure as shown in Fig. 5(a). In this excavation procedure, vertical columns of rock masses from left to right are removed vertically one-by-one. Another excavation method is that the rock mass is horizontally removed through a horizontal layer excavation procedure from top to bottom as shown in Fig. 5(b). Figure 6 is the critical excavation depth when the horizontal layer excavation procedure is implemented. When the excavation depth is only 30 m, a sliding surface has been formed. In order to achieve the critical excavation depth of 35 m, the cohesion of joints must be $c_r = 0.25$ MPa. This difference of the critical excavation depth is caused by the strongly nonlinear process of slope failure in jointed rock slopes. Our numerical simulation shows that the maximum displacement occurs at the top of the excavation surface. The vertical column excavation procedure can remove the most dangerous rock masses in each excavation. This prevents the most dangerous blocks from sliding or toppling, thus producing a higher critical excavation depth. For the horizontal layer excavation procedure, the most dangerous rock mass remains there and the displacements are progressively accumulated. These displacement accumulations behind the
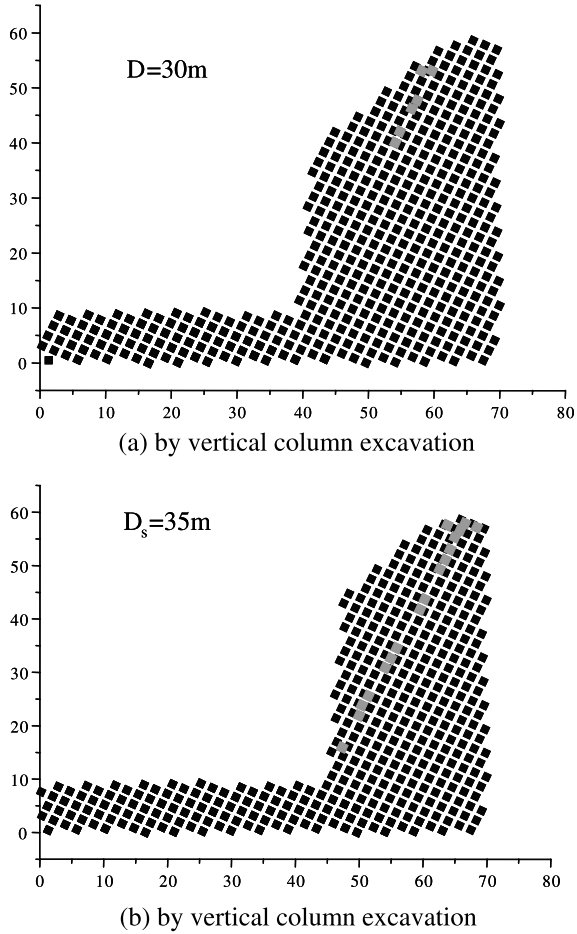
(a) by vertical column excavation

(b) by vertical column excavation

Fig. 4. Sliding point development with vertical column excavation (DEM simulation)

(a) Vertical column excavation   (b) Horizontal layer excavation
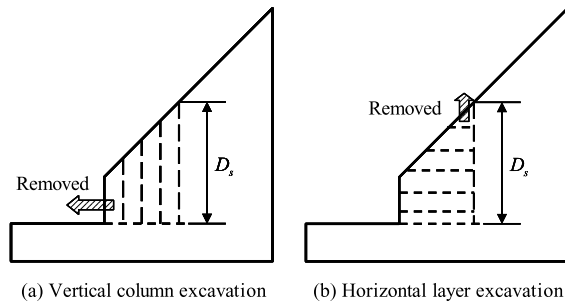
Fig. 5. Two typical excavation procedures

excavation surface speed up the toppling at the top front corner or the formation of a sliding surface, thus producing lower critical excavation depth. These results show that excavation procedure has a crucial effect on the critical excavation depth. For further
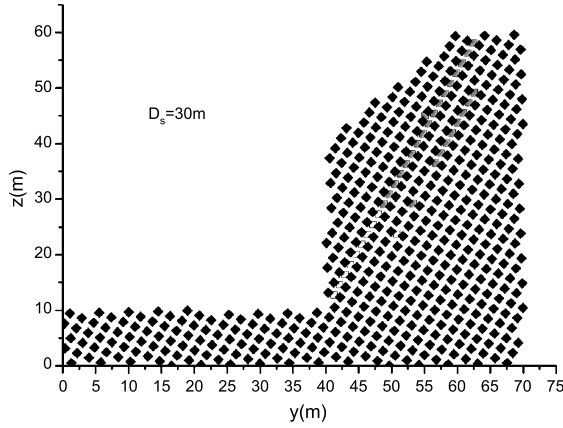
Fig. 6. Sliding point development with horizontal layer excavation (DEM simulation)

study and comparison, only the vertical column excavation procedure is implemented in the hereafter simulations.

4.3 Relationship Between D_s and α

The DEM simulation considers two sets of joints. One is parallel to the sliding surface and the other is perpendicular to the sliding surface. The parameters are taken as $\theta = 65°$, $c_r = 0.2\,\mathrm{MPa}$, and $\phi_r = 30°$ along the sliding surface in the DEM simulations. The joint spacing is assumed to be 2 m. Most slopes in the real projects have the natural slope angles in the range of $40°–70°$. For the LEM the critical excavation depth is $D_s = 54\,\mathrm{m}$ regardless of the number of joints
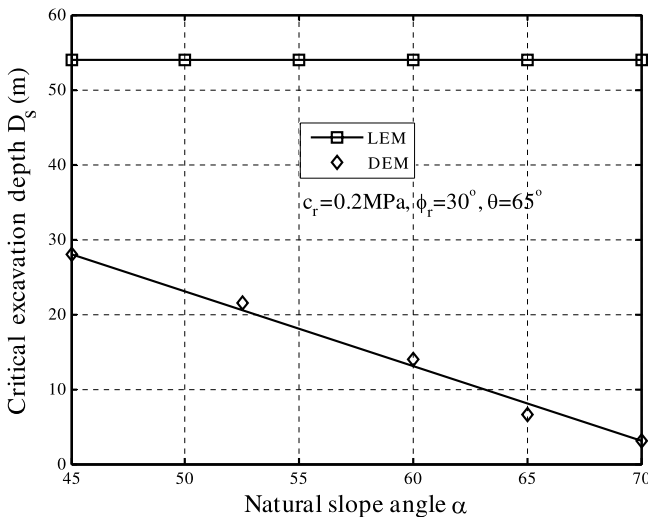
Fig. 7. Critical excavation depth D_s with natural slope angle predicted by DEM and LEM

inside the sliding mass. Figure 7 compares the critical excavation depth when $\alpha \subset (45°, 70°)$ for both LEM and DEM simulations. The critical excavation depth calculated with the DEM decreases with the natural slope angle. This relation is approximated by

$$D_s = 76 - 1.02\alpha. \tag{10}$$

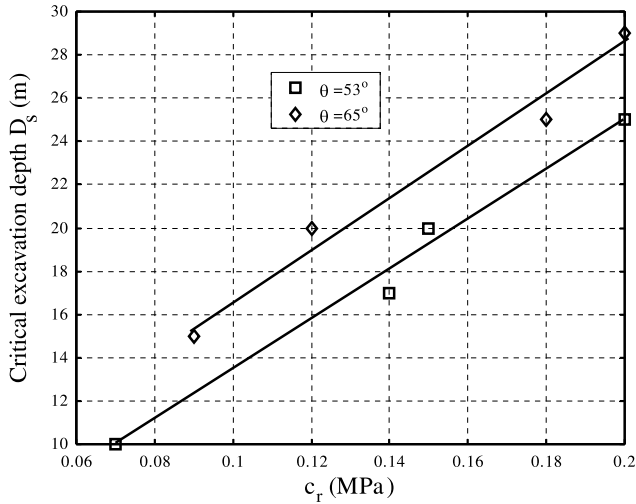The critical excavation depth is much larger for the LEM than for the DEM.

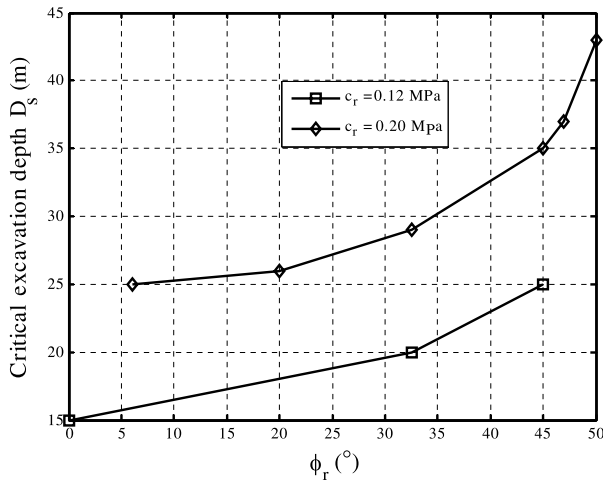**Fig. 8.** Variation of critical excavation depth with joint cohesion c_r (predicted by DEM)

Fig. 9. Variation of critical excavation depth with joint friction angle ϕ_r (predicted by DEM)

4.4 Relationships Between $D_s \sim c_r$ and $D_s \sim \phi_r$

The DEM considers the effects of joint strength on slope stability through Eqs. (4) and (5). Figure 8 compares the curves of the critical excavation depth D_s versus joint cohesion c_r. These curves are calculated with the DEM under two joint inclination angles. The D_s is linear with the cohesion c_r in the range shown in the figure. The higher the c_r, the larger D_s. Figure 9 shows the effect of friction angle on the critical excavation depth calculated by the DEM for $c_r = 0.12$ MPa and 0.2 MPa. The effect of the ϕ_r on slope stability is not as strong as the c_r. For example, if $\theta = 65°$, $\alpha = 45°$, $c_r = 0.12$ MPa, the critical excavation depth D_s changes from 20 m to 15 m when the friction angle ϕ_r varies from 32.5° to 0°. The critical excavation depth reduces slowly with the reduction of friction angle when ϕ_r is lower than 40°.

4.5 Relationship Between D_s and θ

Figure 10 shows another typical jointed rock slope. This slope has a plateau at the top. It may have two potential sliding modes (called as cases 1 and 2) as θ changes. For such a slope, the LEM determines the factor of safety as follows:

In case 1, $\tan\theta \geq \frac{Z_L}{Y_L - d - D_s/\tan\alpha}$, the sliding part is a triangle. The factor of safety F is given by Eq. (8) and the critical excavation depth D_s is given by Eq. (9). That is

$$D_s = \frac{2c_r}{\gamma(\sin\theta\cos\theta - \cos^2\theta\tan\phi_r)}. \tag{11}$$

Differentiating Eq. (11) with θ and letting the derivative be zero, one gets the most dangerous inclination of joints:

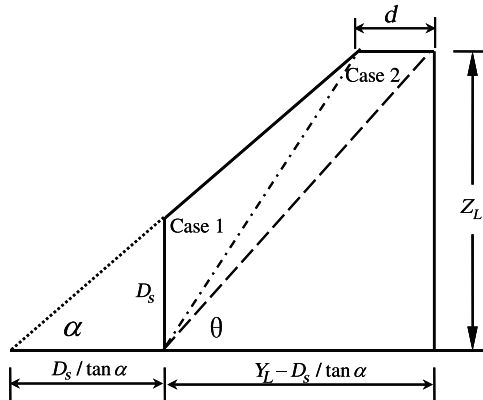$$\theta = \frac{\pi}{4} + \frac{\phi_r}{2}. \tag{12}$$

Fig. 10. Two potential sliding surfaces for a excavation slope

In case 2, $\frac{Z_L}{Y_L - D_s/\tan\alpha} < \tan\theta < \frac{Z_L}{Y_L - d - D_s/\tan\alpha}$, the sliding part is a quadrilateral. The F is obtained as

$$F = \frac{2Z_L\, c_r}{\gamma\sin^2\theta\left[-D^2/\tan\alpha + D(Y_L - d + Z_L/\tan\alpha) + Z_L(Z_L/\tan\theta + d - Y_L)\right]} + \frac{\tan\phi_r}{\tan\theta}.$$

(13)

The critical excavation depth D_s can be obtained when $F = 1$ in Eq. (13). Because this equation is slope size dependent, it is difficult to obtain a closed-form solution for the critical excavation depth. A numerical procedure is employed to calculate the critical excavation depth.

Figure 11 compares the critical excavation depth calculated with the LEM for the above two cases when $\alpha = 45°$, $c_r = 0.2$ MPa, and $\phi_r = 30°$. Although the critical excavation depth varies, the minimum depth is obtained when the joint inclination angle is in $55°$–$65°$. Figure 12 is the critical excavation depth calculated with the DEM for three sets of joints. The results calculated with either LEM (see Fig. 11) or DEM (see Fig. 12) show similar trends, but the DEM predicts smaller critical excavation depth. The difference may be from the joints that are perpendicular to the slope. This set of joints forms a crack behind the sliding part under gravity force (Gokceoglu et al., 2000). Some blocks slide along this crack. Table 1 compares the critical excavation depths and the factors of safety for both LEM and DEM when joint inclination angles are $60°, 65°, 70°$, and $75°$. Their difference is obvious. For example, to the same $F = 1$, the critical excavation depth is 32 m with the DEM and 54 m with the LEM when joint inclination angle is equal to $65°$. The LEM predicts $F > 1.46$ while the DEM already predicts a critical excavation depth. Three sets of joints are selected, but only one is 'critical' to the slope and the other two are parallel to the YZ plane and XZ plane, respectively. Figure 13 compares the critical excavation depths calculated with
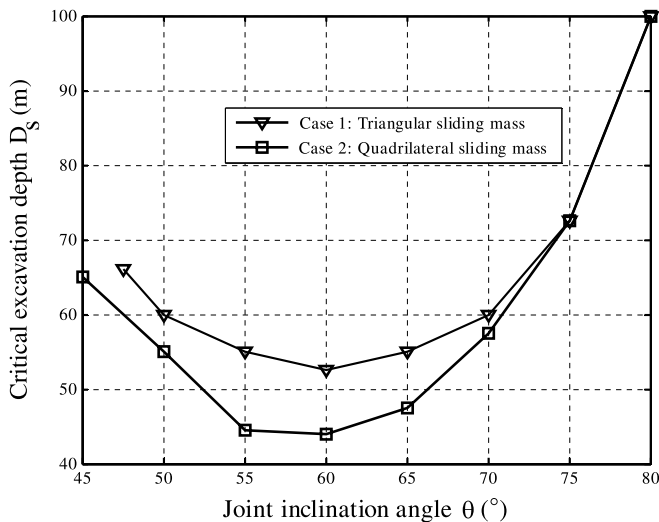

Fig. 11. Variation of excavation depth with joint inclination angle (predicted by LEM)
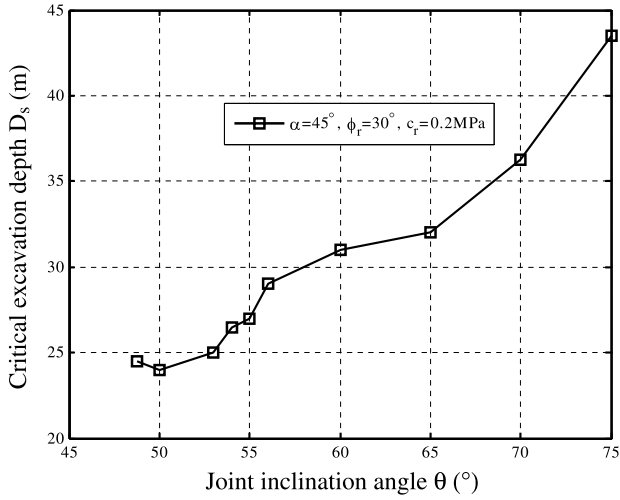
Fig. 12. Variation of critical excavation depth with joint inclination angle (predicted by DEM)

Table 1. Comparison of critical excavation depth and factor of safety of DEM and LEM

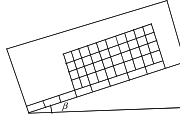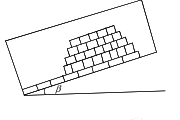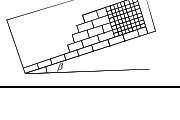| Joint inclination angle θ	60°	65°	70°	75°
Critical excavation depth by the DEM (m)	31	32	36.5	44
Critical excavation depth by the LEM (m)	52.4	54	59	71.5
Factor of safety by LEM at the DEM excavation depth	1.46	1.50	1.49	1.53
Factor of safety by DEM	1.00	1.00	1.00	1.00
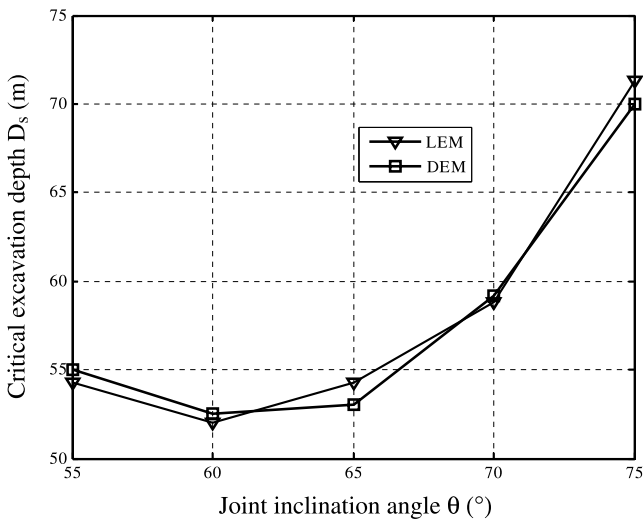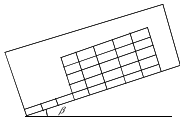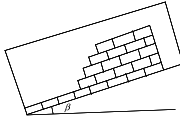
Fig. 13. Critical excavation depths predicted by DEM and LEM for one set of joints

the DEM and LEM of Eq. (9). These two curves are almost identical. This shows that the DEM can give the same excavation depth as the LEM if the same hypotheses are used for the joint structures of the rock slope. In summary, because the DEM can take more sets of joints into consideration, it can go beyond the applicability of the conventional LEM.

5. Joint Structure Effects Observed in Experiments and DEM Simulations

The above-mentioned DEM simulations indicate that the joints in the sliding rock mass may have an important influence on the critical excavation depth of a jointed

Table 2. Experimental cases and their joint configurations

Notation	Joint configuration	Descriptions
Case 1		Big block, persistent joints parallel and perpendicular to bedding surface
Case 2		Big block, stepped joints
Case 3		Medium block, persistent joints
Case 4		Medium block, stepped joints
Case 5		Mixture of different block sizes Front big blocks with stepped joints Back small blocks with persistent joints

Table 3. Geometrical properties of joints

Joint set	Joint angle (degree)		Joint spacing (m)		
	Inclination	Orientation	Big block	Medium block	Small block
1	$90-\beta$	0	0.2	0.1	0.05
2	90	90	0.1	0.1	0.1
3	β	180	0.1	0.1	0.1

Block sizes: $200 \times 100 \times 100 \, mm^3$ (big); $100 \times 100 \times 100 \, mm^3$ (medium); $50 \times 50 \times 50 \, mm^3$ (small)
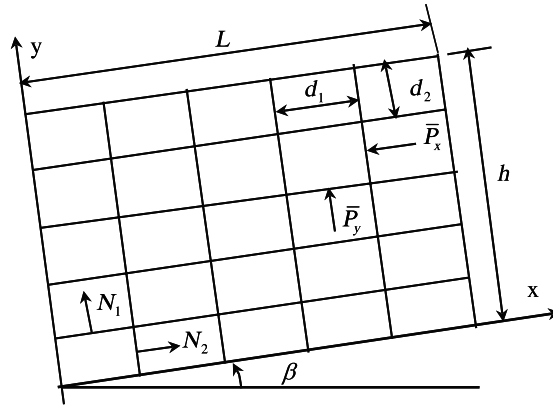
**Fig. 14.** Experiment setup for failure angle of jointed slope

rock slope. If this finding is confirmed by experiments, engineering design criteria should take this joint effect into account. Table 2 lists five artificial jointed rock slopes used in model experiments. These experiments were conducted to study the effect of joint structure on the failure modes of rock slopes. In the experiments, the rock blocks are all made from granite. Three block sizes as given in Table 3 are used to form these five types of artificial jointed rock slopes in laboratory. Cases 1 and 3 have persistent joints parallel and perpendicular to bedding surface as well as a steep front. Cases 2 and 4 have a stepped front and joint structures. Case 5 is a mixture of cases 2 and 3, but the persistent joints are in the back part.

As indicated in Fig. 14, after the blocks have been placed on the test table, the test table is inclined through increasing β until slope failure occurs. The β at slope failure is called the failure angle of this slope. The computational parameters of the interfaces are experimentally determined as $\phi_r = 26°$ and $c_r = 2.14\,\mathrm{Pa}$. Table 4 compares the failure angle obtained by DEM simulations, LEM simulations, and experimental observations. Figure 15 compares the failure modes between the DEM simulations and experimental observations. Figure 15(a) and (b) are for big blocks and stepped joints (case 2), Fig. 15(c) and (d) are for medium blocks and stepped joints (case 4), Fig. 15(e) and (f) are for medium blocks and persistent joints (case 3), and Fig. 15(g) and (h) are the mixture of different block sizes and joints (case 5). It is observed that cases 2 and 4 fail by sliding which is essentially governed by the

Table 4. Comparison of failure angles among experiments, DEM and LEM

Slope type	Case 1	Case 2	Case 3	Case 4	Case 5
Slope details	Big block, unbent joint	Big block, stepped joint	Medium blocks, unbent joint	Medium blocks, stepped joint	Mixture
Experiments (deg)	22.14–24.2	25–26.3	9.8–11.6	23–24.9	19.5–21.8
DEM prediction (deg)	23	25.5	10	23.5	21
LEM prediction (deg)	26	26	26	26	26

friction angle, thus they have similar failure angle. The failure modes for cases 1 and 3 are toppling due to their persistent joints (the photos for case 1 are omitted because they are similar to case 3). Because case 3 has smaller block sizes than case 1, its failure angle is much smaller. This scale effect was also observed by Yoon et al. (2002). Case 5 has a combined failure mode of sliding and toppling, that is, the part with the big blocks slides and the part with the small blocks topples. The small blocks first rotate at the front and then slide in the upper part. This causes the big blocks to slide. The sliding of upper block induces the sliding of big blocks at the lower layers, producing global failure of the slope. These experimental results reveal that joint structures in a rock slope have an important effect on the stability of a jointed rock slope. The figures also indicate that the failure modes in the DEM simulations are in good agreement with experimental observations. The DEM can reasonably predict the failure modes of jointed rock slopes even for different joint structures.
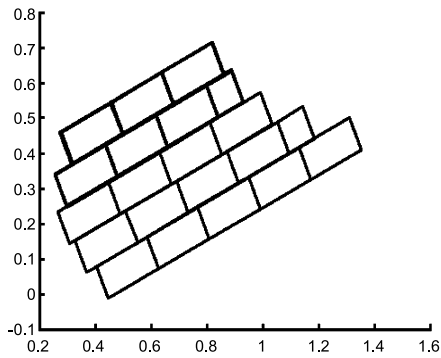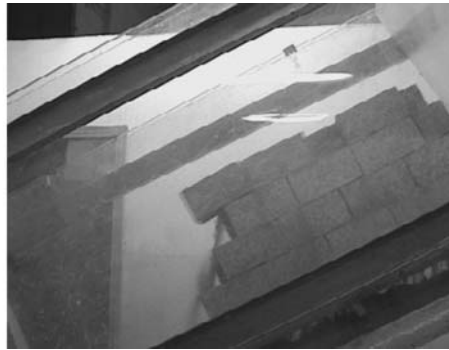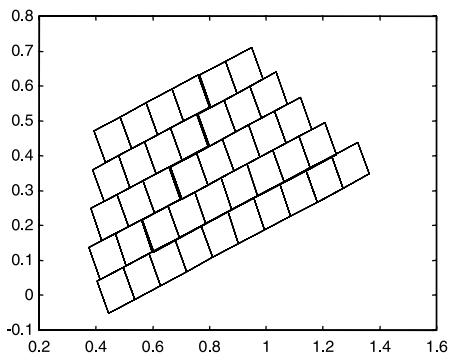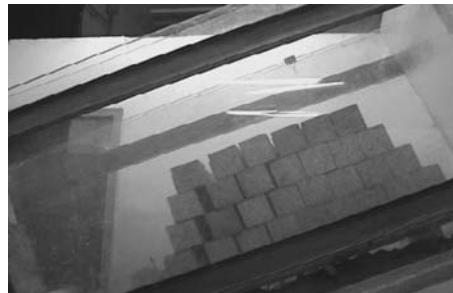

(a) DEM simulation   (b) Experimental observation
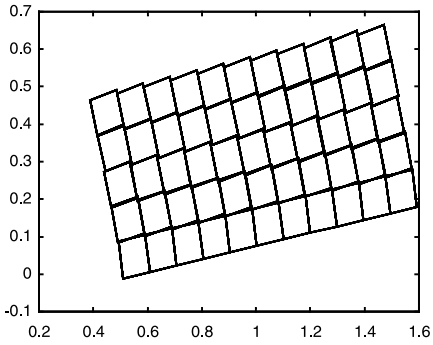
(Big blocks and stepped joints)
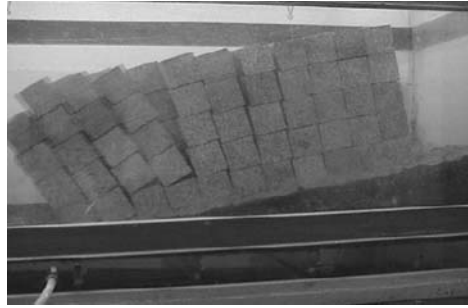

(c) DEM simulation   (d) Experimental observation

(Medium blocks and stepped joints)

Fig. 15. Experimental failure modes of rock slopes with different joint structures and DEM simulations
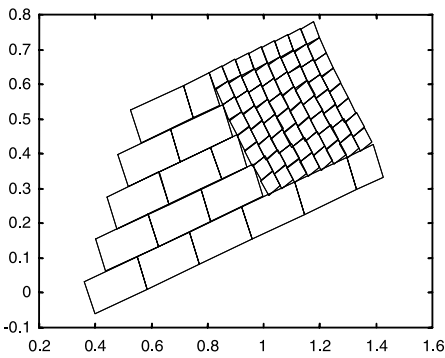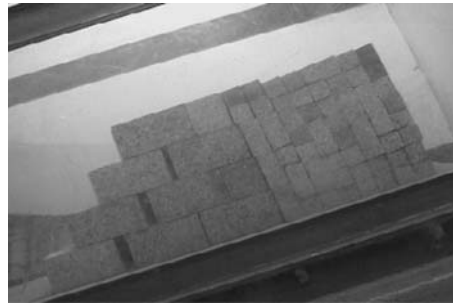
(e) DEM simulation   (f) Experimental observation

(Medium blocks and persistent joints)

(g) DEM simulation   (h) Experimental observation

(Mixture of different block sizes)

Fig. 15 (*continued*)

6. Conclusions

This paper employs a DEM analysis to determine the relationship between critical excavation depth and joint inclination angle, the natural slope angle and the joint strength parameters. The results show that the factor of safety obtained with the DEM can be lower than that obtained with the LEM. This difference appears to come mainly from the consideration of joints not only along the sliding surface but also in other directions. The LEM assumes only one sliding face, whereas the DEM can handle two or three sets of joints and the sliding may occur along any joint. The set of joints, which have the weakest strength or the most dangerous orientation, is critical to the slope stability, but other sets of joints can reduce the integrity of the jointed slope. This reduced integrity can affect the critical excavation depth. If the DEM employs the same joint conditions as the LEM along a sliding surface, similar critical excavation depths are obtained. If a jointed rock slope has more than one failure mode, the LEM cannot describe all multiple failure modes while the DEM can.

Acknowledgements

References

Board, M. (1989): UDEC (Universal Distinct Element Code) Version ICG1.5 Vol.1-3, US, NRC, NUREG/CR-5429, September.

Borri-Brunetto, M., Carpinteri, A., Chiaia, B. (2004): The effect of scale and criticality in rock slope stability. Rock Mech. Rock Engng. 37(2), 117–126.

Chen, W., Li, S. H. (2004): Deformable and breakable block model for 3D distinct element method. Chin. J. Rock Mech. Engng. 23(4), 545–549 (in Chinese).

Chen, Y., Wang, X., Haberfield, C., Yin, J. H., Wang, Y. (2001): A three-dimensional slope stability analysis method using the upper bound theorem. Part I: Theory and methods. Int. J. Rock Mech. Min. Sci. 38(3), 369–378.

Cook, N. G. W. (1992): Natural joints in rock: Mechanical, hydraulic and seismic behaviour and properties under normal stress. Int. J. Rock Mech Min. Sci. Geomech. Abstr. 29(3), 198–223.

Cundall, P. A. (1971): A computer model for simulating progressive large-scale movements in blocky rock systems. In: Proc., Symp. Int. Society for Rock Mechanics, Nancy, France, vol. 1, Paper No. II-8.

Cundall, P. A., Strack, O. D. (1979): A discrete numerical model for granular assemblies. Geotechnique 29(1), 47–65.

Dowding, C. H., Belytschko, T. B., Yen, H. J. (1983): Dynamic computational analysis of opening in joint rock. J. Geotechn. Engng. ASCE 109, 1551–1556.

Dowding, C. H., Dmytryshyn, O., Belytschko, T. B. (1999): Parallel processing for a discrete element program. Comput. Geotechn. 25(4), 281–285.

Dowding, C. H., Belytschko, T. B., Dmytryshyn, O. (2000): Dynamic response of million block cavern models by parallel processing. Rock Mech. Rock Engng. 33(3), 207–214.

Duncan, J. M. (1996): Limit equilibrium and finite element analysis of slopes. J. Geotech. Engng. ASCE 122(7), 577–596.

Gokceoglu, C., Sonmez, H., Ercanoglu, M. (2000): Discontinuity controlled probabilistic slope failure risk maps of the Altindag (settlement) region in Turkey. Engng. Geol. 55(4), 277–296.

Guo, Y. Y., Li, S. H. (2002): Application of DEM in vibration analysis of jointed rock masses under blasting loading. Chin. J. Rock Mech. Engng. 21(Suppl.2), 2408–2412 (in Chinese).

Jing, L. (2003): A review of techniques, advances and outstanding issue in numerical modeling for rock mechanics and rock engineering. Int. J. Rock Mech. Min. Sci. 40(3), 283–353.

Jing, L., Hudson, J. A. (2002): Numerical methods in rock mechanics. Int. J. Rock Mech. Min. Sci. 39(4), 409–427.

Kentli, B., Topal, T. (2004): Assessment of rock slope stability for a segment of the Ankara-Pozanti motorway, Turkey. Engng. Geol. 74(1–2), 73–90.

Kim, K. S., Park, H. J., Lee, S., Woo, I. (2004): Geographic information system (GIS) based stability analysis of rock cut slopes. Geosci. J. 8(4), 391–400.

Li, S. H., Lian, Z. Z., Wang, J. G. (2005): Stability analysis of jointed rock slopes using DEM analysis and physical modeling. Sci. China (Serial E), 48(Suppl.), 1–17.

Low, B. K., Gilbert, R.B., Wright, S. G. (1998): Slope reliability analysis using generalized method of slices. J. Geotechn. Geoenvironm. Eng. ASCE 124(4), 350–362.

Lu, X. B., Li, S. H., Guo, Y. Y. (2002): DEM analysis of response under blast load of the third period longitudinal cofferdam of the Three Gorges. Chin. J. Rock Mech. Engng. 21(2), 159–162 (in Chinese).

O'Connor, K. M., Dowding, C. H. (1992): Distinct element modeling and analysis of mining-induced subsidence. Rock Mech. Rock Engng. 25(1), 1–24.

Wang, J. G., Ichikawa, Y., Leung, C. F. (2003): A constitutive model for rock interfaces and joints. Int. J. Rock Mech. Min. Sci. 40(1), 41–53.

Wang, Y. J., Yin, J. H., Chen, Z., Lee, C. F. (2004): Analysis of wedge stability using different methods. Rock Mech. Rock Engng. 37(2), 127–150.

Wei, Z. A., Li, S. H., Wang, J. G., Wan, L. (2006): A dynamic comprehensive method for landslide control. Engng. Geol. in press.

Yoon, W. S., Jeong, U. J., Kim, J. H. (2002): Kinematic analysis for sliding failure of multi-faced rock slopes. Engng. Geol. 67(1), 51–61.

Authors' address: Dr. J. G. Wang, Tropical Marine Science Institute, National University of Singapore, Singapore 119260; e-mail: tmswjg@nus.edu.sg